International Food Research Journal 27(1): 182 - 196 (February 2020)
Journal homepage: *http://www.ifrj.upm.edu.my*

New thin-layer drying models for the design and simulation of cassava root dryers and phenomenological study of interaction water-starch during diffusion

[1]*Faneite, A. M., [1]Parra, J., [1]Colón, W., [2]Ferrer, A., [3,4]Angós, I. and [5]Argüello, G.

[1]Laboratorio de Ingeniería Química "Prof. Ydelfonso Arrieta", Escuela de Ingeniería Química, Facultad de Ingeniería, Universidad del Zulia. Maracaibo, Venezuela
[2]Departamento de Química, Facultad Experimental de Ciencias, Universidad del Zulia. Maracaibo, Venezuela
[3]Facultad de Ciencia e Ingeniería en Alimentos, Universidad Técnica de Ambato, Campus Huachi. Ambato, Ecuador
[4]Department of Agricultural Engineering, Biotechnology and Food, Public University of Navarre, Pamplona, Spain
[5]Instituto Nacional de Investigaciones Agrícolas (INIA). Trujillo, Venezuela

Article history

Received: 18 February 2017
Received in revised form: 23 October 2019
Accepted: 25 November 2019

Keywords

desorption, kinetic modelling, effective diffusivity, pseudo equilibrium, moisture content

Abstract

In the present work, drying phenomenology of cassava root slices was studied at 55, 65, 75, 85, 95, 105 and 115°C, and at 5- and 6-mm thicknesses. Chemical analysis, X-ray diffraction (XRD) measurements, and Fourier-Transform Infrared Spectroscopy (FTIR) of samples of cassava, dried at different temperatures, were carried out. Additionally, the performance of three new thin-layer drying kinetics models was analysed. Initial moisture in a wet basis and starch content in a dry basis were 62.4 and 74.8%, respectively. The drying curves showed a monotonic decrease in time and a progressive closeness as the drying temperature increased (with the exception of 115°C), reaching a stage, so-called, dynamic pseudo-equilibrium, located between the typical storage moisture content, and the real equilibrium. Drying rate curves showed a single stage of decreasing drying rate with internal control, while desorption curves showed a sigmoidal characteristic shape of an anomalous diffusion type, confirmed by the potential behaviour of the effective diffusivity with respect to the material moisture content. The 115°C drying curve behaviour was explained by the changes seen in XRD patterns and FTIR spectra. The new Modified-Faneite-Suárez model got an extraordinary performance modelling the cassava drying, while Faneite-Mosquera model got a very good performance and the most recommendable to be used in design and simulation of cassava dryers based on its sound theoretical basis and prediction capabilities in a broad spectrum of temperatures.

Introduction

Venezuelan production of cereals destined to feed livestock is very deficient. Yellow corn importations averaged $2.3 \cdot 10^6$ tons/year, between 2013 and 2016, while production has been decreasing, averaging $1.9 \cdot 10^6$ tons/year in the same period, thus subtracting security and food sovereignty to the country (FAO, 2017; USDA, 2018) due to several factors (García *et al.,* 2009). One possible solution to this situation is to seek locally produced crops as potential substitutes of corn like cassava, a starch-rich source with a low content of fibre, whose use is convenient as broiler, swine, and other non-ruminant's compound feeding stuffs.

Several studies have demonstrated that cassava roots and leaves are suitable to be used as an appropriate alternative energetic and protein sources in cattle, swine, and poultry feeding; in the form of flour or silage (Garzón, 2010). One of the main problems in postharvest handling of cassava is the rapid spoilage due to the high water content of the roots. This makes it essential to carry out a previous drying treatment before the product storage, to obtain a long period of shelf life and minimising the extent of microbial decomposition (Durango *et al.,* 2004).

In the last decades, extensive studies have been carried out to determine the kinetics of experimental drying of the cassava root. This task has been mainly focused within a narrow temperature range between 35 and 70°C, given its high initial humidity between 75.4 and 61% on a wet basis (Salgado *et al.,* 1994; Kajuna *et al.,* 2001; Carranza and Sánchez, 2002; Hernández-Pérez *et al.,* 2004; Salcedo *et al.,* 2014). Except for Kajuna *et al.* (2001) who worked with cubes and Hernández-Pérez *et al.* (2004) who worked with parallelepipeds, both diffusing on all faces, the rest of the authors worked with thin layers, ranging between 2 and 20 mm. Only Salgado *et al.* (1994) conducted studies controlling the relative

*Corresponding author.
Email: afaneite@fing.luz.edu.ve

humidity of the air in the drying chamber.

Considering the generation of models for the simulation and design of industrial dryers, the available information is very sparse in this regard. Salgado *et al.* (1994), Kajuna *et al.* (2001) and Salcedo *et al.* (2014) reported empirical modeling, recommending Newton, Page, and approximate Diffusion as the best models. Among them, only Salgado *et al.* (1994) reported a model for the Newton parameter, obtained by linear regression, dependent on the initial moisture of the product, the linear velocity of the air, and the gas temperature; while the other two works reported parameters for each evaluated condition. Carranza and Sánchez (2002) only reported the phenomenological study of the drying process, while Hernández-Pérez *et al.* (2004) reported the use of a neural network for the generation of a kinetic model, dependent on air temperature, air velocity, shrinkage, time, and air humidity. Regarding semi-theoretical modeling, only Salcedo *et al.* (2014) reported activation energies for comparative effects between the evaluated conditions and other materials, and a linear correlation of the effective diffusivity, dependent on the conditions evaluated.

A main disadvantage of the works of Salgado *et al.* (1994) and Salcedo *et al.* (2014) is that the models obtained apply exclusively to the evaluated drying conditions (gas temperature between 35-70°C and linear gas velocities between 1-3 $m \cdot s^{-1}$). The same applies for the model of Hernández-Pérez *et al.* (2004) due to the complete empirical character of the models based on artificial neural networks. The problem with this approach gets worse due to the fact that it applies to parallelepipedic pieces of cassava, being the same for the cubic figures of Kajuna *et al.* (2001). Without a three-dimensional modeling based on the second Fick law applied to all the faces where moisture diffuses, these models have a very limited capacity of prediction in cassava pieces of those specific geometric shapes.

Véliz *et al.* (2002) and Zomahoun *et al.* (2005) reported the sun drying of cassava and the drying in a solar dryer, respectively, but information about the drying process, useful in designing industrial or semi-industrial dryers, are not yet available.

The main objectives of the present work were to determine the potential of cassava roots as an animal feed production energy source at industrial scale and the performance of a new empirical thin-layer drying model and a new semi-theoretical model tested against the empirical models available, making use of the Activation Energy as a modeling parameter.

Materials and methods

Sampling

Roots of cassava (*Manihot esculenta* Crantz) were harvested between February and September 2010 in the Farm Los Salas, in the State of Zulia (Venezuela). Upon receiving, cassava roots were washed to eliminate any residual dirt, and stored with external skin in sealed plastic bags at 2°C until further analysis.

Chemical characterisation of the raw material

For initial moisture content, triplicate samples of 200 g of cassava roots were weighed in Adventure™ analytical balance (OHAUS, USA) and introduced into a convective oven (Memmert 854, Germany) at 105°C until constant weight was reached.

Kjeldhal method was used to assess the raw protein content of cassava roots. After this process, cassava roots were dried at 55°C, grinded and defatted using Soxhlet method for starch determination. Ash was determined using method 942.05 - ash of animal feed (AOAC, 2000). Van Soest method was used to separate the cellular wall content into four fractions: Neutral Detergent Fibre (NDF), Acid Detergent Fiber (ADF), Acid Detergent Lignin (ADL), and Van Soest ash (VSa), expressed in percentages (AOAC, 2000).

Thin layer drying kinetics

The weight of three replicate samples were measured at the beginning (m_0 = 29.4877 ± 1.4024 g) and at intervals of 3 or 5 min in an analytical scale Adventure™ (OHAUS, USA), for seven air temperatures (55, 65, 75, 85, 95, 105 and 115°C) and two layer heights (5 and 6 mm). Replicates were placed in aluminium plates of 10 × 9.5 cm without grids, in such a way that diffusion took place on a single face. Temperatures were previously set in a hot air steriliser oven model 3475M (Samford, USA). Samples were weighed at each interval until a constant weight was verified in less than 1 mg. Dry mass were measured in a Thermo Fisher Scientific oven model 6528 (Dubuque, USA) at 105°C for 24 h, being their initial moisture in the range of 60.59 ± 2.29% on a wet basis (wb). The relative humidity and laboratory temperature during the experiments were in the range of 70.47 ± 2.07% and 21.44 ± 1.09°C, respectively.

Processing and presentation of kinetic data

Initial moisture content and moistures on dry basis, for each experimental point of the triplicates of the 14 experiments were calculated using Eq. 1:

$$X_0 = \frac{m_0}{m_{DS}},\ X_t = \frac{m_t}{m_{DS}} \quad \text{(Eq. 1)}$$

where, m_0 = initial mass in g; m_t = mass in time (t) in g; m_{DS} = mass of the dry solid in g (after 24 h at 105°C); X_t = dry basis moisture in time (t) in kg_{water}·kg_{DS}^{-1}; X_0 = initial moisture in kg_{water}·kg_{DS}^{-1}.

Once the humidity (dry basis) was calculated, the average drying curves were represented in terms of X_t / X_0 *versus t*, to identify on one hand, any incongruent behaviour with respect to drying, especially in the curves with the highest temperatures; and on the other hand, the beginning of the dynamic pseudo-equilibrium period (Faneite *et al.,* 2016). This was done to establish the moisture of dynamic pseudo-equilibrium (X_{dpe}), which is the point where the monotonic decrease of the drying curve changes abruptly to a condition of a very slow decrease in humidity.

Qualitative analysis of the drying process

Once identified, the X_{dpe} points in the drying curves, in terms of X_{dpe} / X_0, and the kinetic drying curves with an incongruent behaviour by starch reactions at high temperatures discarded, kinetics drying data were plotted in terms of M_R *versus t*, using Eq. 2.

$$M_R = \frac{X_t - X_{dpe}}{X_0 - X_{dpe}} = \frac{X_t/X_0 - X_{dpe}/X_0}{1 - X_{dpe}/X_0} \quad \text{(Eq. 2)}$$

where the terms of Eq. 2 were the same with Eq. 1.

Moisture of dynamic pseudo-equilibrium period (X_{dpe}) has been defined by Faneite *et al.* (2016) as the moisture at the beginning of the dynamic pseudo-equilibrium period of drying (DPE). This period is observed between the normal monotonic behaviour seen in traditional drying curves and the thermodynamic equilibrium moisture (X_e), and is a function of the air temperature and relative humidity. During this period, water loss speed of the material being dried is extremely slow, and it could be confounded with X_e. The term "dynamic" is used due to the fact that the beginning of this period is determined in the same experiment of drying where the air flows through or onto the sample. X_{dpe} is described by Faneite *et al.* (2016) as the drying limit in economic terms, because it is lower than the storage moisture, and it can be easily identified and measured. For these reasons, it is considered convenient to be included in the calculations of kinetic equations instead of X_e.

According to Faneite (2010), drying curves in terms of M_R *versus t*, were then smoothed prior to the determination of velocity, using a 6th order polynomial (Eq. 3), with the option of tendency line of the graphic editor of Excel®.

$$M_R = a \cdot t^6 + b \cdot t^5 + c \cdot t^4 + d \cdot t^3 + e \cdot t^2 + f \cdot t + g \quad \text{(Eq. 3)}$$

where *a-g* = empirical coefficients of Eq. 3.

For the determination of the drying rate curves, the polynomials obtained for each drying curve were derived as a function of t (Eq. 4).

$$\frac{dM_R}{dt} = 6a \cdot t^5 + 5b \cdot t^4 + 4c \cdot t^3 + 3d \cdot t^2 + 2e \cdot t + f \quad \text{(Eq. 4)}$$

where the terms of Eq. 4 were the same as for Eq. 3. Finally, drying rate curves were made by plotting $-dM_R/d_t$ (Eq. 4) *versus* M_R (Eq. 3) as continuous lines.

To construct the water desorption curves, the entire drying kinetics data were smoothed (without the discarded curves) in terms of X_t/X_0 *versus t*, just as M_R, with the Eq. 5.

$$\frac{X_t}{X_0} = a' \cdot t^6 + b' \cdot t^5 + c' \cdot t^4 + d' \cdot t^3 + e' \cdot t^2 + f' \cdot t + g' \quad \text{(Eq. 5)}$$

where *a´, b´, c´, d´, e´, f´* and *g´* = empirical coefficients of Eq. 5.

The ratio of the accumulated mass of water desorbed in time 0 (amw_0), divided by the total water desorbed when time goes to infinity (amw_∞), is 0. The rest of the points were calculated with Eq. 12. Deduction of these equations is as follows:

$$\frac{amw_t}{amw_\infty} = \frac{m_{t-1} - m_t + amw_{t-1}}{amw_\infty} \quad \text{(Eq. 6)}$$

$$\frac{amw_t}{amw_\infty} = \frac{m_{t-1} - m_t}{amw_\infty} + \frac{amw_{t-1}}{amw_\infty} \quad \text{(Eq. 7)}$$

$$amw_\infty \approx mw_0 \quad \text{(Eq. 8)}$$

$$\frac{amw_t}{amw_\infty} = \frac{m_{t-1} - m_t}{mw_0} + \frac{amw_{t-1}}{amw_\infty} \quad \text{(Eq. 9)}$$

$$\frac{amw_t}{amw_\infty} = \frac{m_{t-1}}{mw_0} - \frac{m_t}{mw_0} + \frac{amw_{t-1}}{amw_\infty} \quad \text{(Eq. 10)}$$

$$\frac{amw_t}{amw_\infty} = \frac{m_{t-1}/m_{DS}}{mw_0/m_{DS}} - \frac{m_t/m_{DS}}{mw_0/m_{DS}} + \frac{amw_{t-1}}{amw_\infty} \quad \text{(Eq. 11)}$$

$$\frac{amw_t}{amw_\infty} = \left(\frac{X_{t-1}}{X_0} - \frac{X_t}{X_0}\right) + \frac{amw_{t-1}}{amw_\infty} \quad \text{(Eq. 12)}$$

where, *amw* = accumulated mass of water in g; *mw* = mass of water in g; *m* = mass of solid that dries in g; *X*, = the moisture of the solid on a dry basis in $kg_{water} \cdot kg_{DS}^{-1}$; subscript *0* = initial; *t* = a discrete point corresponding with a time *t*; *t-1* = a discrete point of a time before *t*; ∞ = infinity time, when the solid that dries, reaches equilibrium moisture.

Smoothed data of (amw_t/amw_∞) were plotted versus the square root of time, as a continuous line. The shape of these curves was then compared with the classification of Rogers (Crank, 1975).

Effective diffusivity curves are a simple qualitative tool proposed to identify change processes in the chemical nature, microstructure, crystallinity and the interactions of the components of a material being dried, especially in polysaccharide-based materials that contain mainly pectin, starch or cellulose. A material, whose components do not show interactions with water and do not change during the diffusion of water to the surface, will present an effective diffusivity independent of the moisture content. If the behaviour of the effective diffusivity curve is potential, as shown by Faneite *et al.* (2016), an exponent close to 0 will result in a more fickianity during the drying process of the material under study. The tool was not conceived to find possible deviations of the perfect linear behaviour of an experimental drying dataset, when plotting it in traditional terms of $\ln M_R$ *versus t*, neither to calculate exact values of effective diffusivity. Instead, with the use of this tool, it is expected to find tendencies different to the linear one. It is clear that, if an experimental dataset has a linear behaviour, the linear model of adjustment will have a better adjustment and statistical significance than more complex mathematical expressions. A "fickian" material must show a horizontal effective diffusivity curve, parallel to the moisture ratio axis. The physical evidence of a possible non-fickian diffusion is the shrinkage, that when it is adjusted to a mathematical expression, will allow the authors to avoid the hard effort to determine the expression of effective diffusivity, integrating the deviation of the diffusivity into the shrinkage expression (Karim and Hawlader, 2005). Other authors find expressions of shrinkage and diffusivity, taking for granted the fact that, this kind of material does not have a constant effective diffusivity (Esmaiili *et al.,* 2007). Mayor and Sereno (2004) presented an important compilation of equations of shrinkage in the drying process.

On the other hand, comparing the wide array of effective diffusivity curves for different materials, we can appreciate the appearance of "families" in terms of similar water affinity (hygroscopicity) or water diffusion barriers. In the past, some authors tried to find an explanation for these affinities by making use of the parameter energy of activation, but they did not obtain sound conclusions in phenomenological terms. However, there are some similarities between these tools with respect to the determination of the energy of activation (*Ea*). The last one comes from a plot of $\ln M_R$ *versus t*; and in the first one, the plot is made with M_R and *Deff* as a function of *t*, *L* in case of to be measured during the drying experiment, and the same M_R. Both methods make assumptions which reduce their theoretical exactitude: in the case of the energy of activation, a linear association between $\ln M_R$ and *t*, or the use of the ideal gas constant, conceptually created for very different uses. In the case of effective diffusivity curves, the use of a mathematical solution for processes with constant effective diffusivity (Crank solution of second Fick Law) is used to determine its variation. In short, we consider that this tool proposes an interesting alternative to *Ea* for the uses explained earlier, given the scientific evidence of the non-constant relationship of the effective diffusivity with respect to the moisture content in a drying process (Marousis *et al.,* 1991; Aguerre and Suarez, 2004).

Effective diffusivity was calculated at each point of the smoothed data, using the solution of Crank to the second Fick's law of diffusion (Eq. 15), and then plotted in function of M_R.

$$M_R = e^{\left(-\frac{\pi^2 \cdot Deff \cdot t}{L^2}\right)} \quad \text{(Eq. 13)}$$

$$-lnM_R = \frac{\pi^2 \cdot Deff \cdot t}{L^2} \quad \text{(Eq. 14)}$$

$$Deff = \frac{-L^2 \cdot lnM_R}{\pi^2 \cdot t} \quad \text{(Eq. 15)}$$

where, M_r = moisture fraction; *Deff* = effective diffusivity in $m^2 \cdot s^{-1}$; *L* = layer thickness (m); and t = time in s.

The representation of the entire set of curves of this sub-section was made with 677 smoothed points.

X-ray diffraction (XRD) and Fourier Transform Infrared (FTIR) spectroscopy

XRD was carried out in the *2θ* range from 8 to 40° on powdered samples dried at 55, 95 and 115°C until reaching less than 10% moisture (wet basis). A Brucker D8 diffractometer (Karlsruhe, Germany) was used for these determinations. For FTIR, a sample of 3 mg was used in spectrum determinations carried out in a Shimadzu IRPrestige-21

spectrophotometer (Portland, USA) using the 400 - 4000 cm^{-1} wave number range and using the diffuse reflectance mode setting. The applications of these two analytical techniques seek to find changes in the chemical composition, para-crystallinity or the structure of the material during the drying process.

Crystallinity index by XRD

Samples were analysed in the 2θ range of 8 - 40°. Crystallinity of samples was calculated quantitatively following the procedure suggested by Nara and Komiya (1983). A smooth curve was plotted connecting the base of each peak, between 8.49 and 28.94° of 2θ. The area of the peak over this curve corresponded to the crystalline area (*Ca*). The area comprised between the curve and a baseline connecting the points with 2θ intensity 8.49 and 28.94°, corresponded with the amorphous area (*Aa*) (Cheetham and Tao, 1998).

The areas were calculated using the Simpson's 1/3 rule and the Crystallinity index (*CrI*) using Eq. 16:

$$\%CrI = \frac{Ca \cdot 100\%}{Ca + Aa} \quad \text{(Eq. 16)}$$

where, *Ca* = crystalline area; and *Aa* = amorphous area, both in the same units of area.

FTIR analysis of infrared spectrum

In order to generate the Fast Fourier Transform of the infrared spectra from the analysed material, the absorbance (%) was plotted as a function of wave number (cm^{-1}). Finally, crystallinity index was calculated by means of the absorbance ratio between the 1042 and 1022 cm^{-1} band as proposed by Smits *et al.* (1998).

Modelling of thin layer drying kinetics

Nine empirical equations (Eq. 17 - 25) and two semi-theoretical models (Eq. 26 and 36) were tested for modelling the thin layer drying kinetics data following, partially, the procedure of Faneite (2010). The models Newton or Lewis, Exponential of two terms, Approximate diffusion, Verma, Page, Modified Page, Modified-Faneite-Suárez (Guillén *et al.,* 2017), Logistic, and Gauss (Faneite, 2010) corresponded to Eq. 17 - 25, respectively. Empirical thin-layer drying equation with potential to generate negative tails in the final part of the drying curves (e.g. Logarithmic or Midilli equation) were discarded.

$$M_R = e^{-k \cdot t} \quad \text{(Eq. 17)}$$

$$M_R = a \cdot e^{-k \cdot t} + (1 - a) \cdot e^{-k \cdot a \cdot t} \quad \text{(Eq. 18)}$$

$$M_R = a \cdot e^{-k \cdot t} + (1 - a) \cdot e^{-k \cdot b \cdot t} \quad \text{(Eq. 19)}$$

$$M_R = a \cdot e^{-k \cdot t} + (1 - a) \cdot e^{-g \cdot t} \quad \text{(Eq. 20)}$$

$$M_R = e^{-k \cdot t^n} \quad \text{(Eq. 21)}$$

$$M_R = e^{-(k \cdot t)^n} \quad \text{(Eq. 22)}$$

$$M_R = a \cdot e^{-k \cdot t^n} + (1 - a) \cdot e^{-g \cdot t^n} \quad \text{(Eq. 23)}$$

$$M_R = b/\left(1 + a \cdot e^{k \cdot t}\right) \quad \text{(Eq. 24)}$$

$$M_R = a \cdot e^{-\frac{(t+b)^2}{2c^2}} \quad \text{(Eq. 25)}$$

where, M_R = moisture fraction; t = time; *a, b, c, g, k,* and n = parameters of empirical equations.

The parameters of the models were calculated using Excel® Solver by means of GRG-Nonlinear method and Least Squares method with smoothed data. Faneite-Suárez thin-layer drying equations (Guillén *et al.,* 2017) is based on Hii model changing the pre-exponential factors for the type Exponential of two terms model, Approximate diffusion model, or Verma model, in order to ensure a value for M_R of 1 in time 0, with the addition of the proportional term of Midilli model. First modification comprised the elimination of the proportional term "*bt*" to avoid finding negative predicted moistures at the end of the kinetics step. Eq. 25 is inspired in the Gaussian function, due to the similarity between the drying curve and a tail of the Gaussian bell curve (same family of the Logistic equations).

Although Solver tool automatically removes any non-significant parameter in the iterative process, non-linear regression with Marquardt's method was also used to determine the significance of the parameters of the Modified-Faneite-Suárez and Gauss equations. This latter process was conducted by means of Statgraphics Centurion XV software, setting a 95% of confidence.

Eq. 26 is the typical drying kinetics expression with energy of activation (E_a) and the independent term of the Arrhenius equations of the effective diffusivity (D_0), as main parameters. Smoothed data of $\ln M_R$ *versus t* was plotted and adjusted to a straight line with of Excel® Solver, specifying a value of 1 in the tendency line for t = 0. Absolute value of *Deff* was obtained from the slopes, equalling *Deff* to $slope \cdot L^2 \bullet \pi^{-2}$, for each temperature. $\ln Deff$

were plotted in function of *1/T* (1/K), and equally adjusted to a straight line, with of Excel® Solver. The independent term of the tendency line was lnD_0 and the slope *Ea/R* as in Eq. 26:

$$M_R = e^{\left\{-\frac{\pi^2 \cdot D_0 \cdot e^{\left[-\frac{E_a}{R\cdot(T+273,15)}\right]} \cdot t}{L^2}\right\}} \quad \text{(Eq. 26)}$$

where, M_R = moisture fraction; t = time in s; D_0 = independent term of the Arrhenius equation of the effective diffusivity in m²•s; E_a = energy of activation in kJ•kg•mol^{-1}; R = ideal gas constant with a value of 8.3144 kJ•kg•mol-*1*•K-*1*.

Following the procedure of Faneite and Mosquera (personal communication), smoothed data of *Deff* (Eq. 15) *versus* lnM_R was plotted and adjusted to a straight line of tendency with the graphic editor of Excel®. Independent terms and slopes were obtained from the mathematical expression with the same tool. This semi-theoretical method was combined with the mathematical expression of X_{ped} / X_0, using Eq. 2, resulting in Eq. 36. This model was created to have a semi-theoretical expression with a high accuracy useful in simulation of industrial dryers, with parameters easily adjustable with the temperature.

$$Deff = b + m \cdot lnM_R \quad \text{(Eq. 27)}$$

$$M_R = e^{\left[-\frac{\pi^2 \cdot (b+m\cdot lnM_R)\cdot t}{L^2}\right]} \quad \text{(Eq. 28)}$$

$$lnM_R = -\frac{\pi^2 \cdot (b+m\cdot lnM_R)\cdot t}{L^2} \quad \text{(Eq. 29)}$$

$$lnM_R \cdot L^2 = -\pi^2 \cdot b \cdot t - \pi^2 \cdot m \cdot lnM_R \cdot t \quad \text{(Eq. 30)}$$

$$lnM_R \cdot L^2 + \pi^2 \cdot m \cdot lnM_R \cdot t = -\pi^2 \cdot b \cdot t \quad \text{(Eq. 31)}$$

$$(L^2 + \pi^2 \cdot m \cdot t) \cdot lnM_R = -\pi^2 \cdot b \cdot t \quad \text{(Eq. 32)}$$

$$lnM_R = -\frac{\pi^2 \cdot b \cdot t}{L^2 + \pi^2 \cdot m \cdot t} \quad \text{(Eq. 33)}$$

$$M_R = e^{-\frac{\pi^2 \cdot b \cdot t}{L^2 + \pi^2 \cdot m \cdot t}} \quad \text{(Eq. 34)}$$

$$M_R = \frac{X_t/X_0 - X_{dpe}/X_0}{1 - X_{dpe}/X_0} = e^{-\frac{\pi^2 \cdot b \cdot t}{L^2 + \pi^2 \cdot m \cdot t}} \quad \text{(Eq. 35)}$$

$$X_t/X_0 = X_{dpe}/X_0 + \left(1 - X_{dpe}/X_0\right) \cdot \left(e^{-\frac{\pi^2 \cdot b \cdot t}{L^2 + \pi^2 \cdot m \cdot t}}\right) \quad \text{(Eq. 36)}$$

where, X_t = moisture in time t in a db in kg_{water}•kg_{DS}^{-1}; X_0 = initial moisture content in a db in kg_{water}•kg_{DS}^{-1}; X_{ped} = moisture of the beginning of the dynamic pseudo-equilibrium stage in a db in kg_{water}•kg_{DS}^{-1}; t = time; b and m = parameters of Faneite-Mosquera model.

Experimental and smoothed modelled data were plotted together and residuals (R) of M_R or X_t / X_0 calculated with Eq. 37.

$$R = M_{R_{exp}} - M_{R_{pred}} \text{ or } R = (X_t/X_0)_{exp} - (X_t/X_0)_{pred} \quad \text{(Eq. 37)}$$

where, *exp* and *pred* = experimental and predicted points, respectively. The rest of variables have been explained previously. Models with a poor adjustment to the experimental behaviour or a biased distribution of residuals were discarded.

The final selection of the best model was done using analytic statistical criteria of selection. Following the selection method of Faneite *et al.* (2016), results of coefficient of determination (R^2), model efficiency (η_m), root mean square error (RMSE), and Chi-square (χ^2) (Eq. 38, 39, 40 and 41, respectively), for each temperature, were considered as replicates and each evaluated model as treatments, in an ANOVA and LSD test with 95% of confidence. Model with a value of R^2 and η_m of 1 indicated a perfect follow-up of the trend of experimental data by the model. Values of *RMSE* and χ^2 of 0 indicated a model without bias with respect to the experimental points.

$$R^2 = 1 - \frac{\sum_{i=1}^{N}\left(V_{pred,i} - V_{exp,i}\right)^2}{\sum_{i=1}^{N}\left(V_{pred,prom} - V_{pred,i}\right)^2} \quad \text{(Eq. 38)}$$

$$\eta_m = \frac{\sum_{i=1}^{N}\left(V_{exp,i} - V_{exp,prom}\right)^2 - \sum_{i=1}^{N}\left(V_{pred,i} - V_{exp,i}\right)^2}{\sum_{i=1}^{N}\left(V_{exp,i} - V_{exp,prom}\right)^2} \quad \text{(Eq. 39)}$$

$$RMSE = \sqrt{\frac{\sum_{i=1}^{N}\left(V_{exp,i} - V_{pred,i}\right)^2}{N}} \quad \text{(Eq. 40)}$$

$$\chi^2 = \frac{\sum_{i=1}^{N}\left(V_{exp,i} - V_{pred,i}\right)^2}{N - n} \quad \text{(Eq. 41)}$$

where, V = M_R or X_t / X_0 depending on the case; *exp* and *pred* = experimental, and predicted data for each model, respectively; i = number of an experimental or predicted drying point; N = number of experimental points evaluated; n = number of parameters of the model; the rest of the variables have been explained previously.

Results and discussion

Chemical characterisation of the cassava roots

Moisture content of the cassava roots (Table 1) implies a drying process to avoid microbial and enzymatic degradation in agro-industrial plants with an installed capacity much lower that the harvest peak production, where cassava roots are an important raw material of these plants.

Proximate chemical characterisation was in the same order of magnitude reported by Carranza and Sánchez (2002). Starch resulted as the main component of cassava roots (Table 1). Drying is a process of desorption of a solvent (water) inside a polymeric matrix (starch) with chemical affinity to this solvent. Accordingly, it could be predicted, that the drying of the cassava roots is a non-fickian diffusion process. In this process, the biopolymer matrix changes continuously its diffusivity coefficient to the extent that water diffuses. Van Soest analysis showed the presence of some different components of starch. First component (reducing sugars) was contained in the soluble fraction, together with solubilised proteins, lipids and a fraction of the total ash. The second component of starch, with some recalcitrance, was suspended with an acid solution, and represented as hemicellulose. Finally, insoluble cellulose and lignin fraction represent the fibre of a proximate analysis.

Table 1. Chemical characterization of cassava root.

Parameter	Value	
	Mean	SD
Initial moisture (%, wb)		
initial moisture (*M*)	62.40	0.03
dry matter (*DM*)	37.60	(*)
Proximate analysis and starch (%, db)		
starch	74.80	0.66
nitrogen-free extracts (*NFE*)	87.24	(*)
ash (*A*)	6.69	0.57
crude protein (*CP*)	3.67	0.32
crude lipid (*CL*)	0.11	0.01
crude fibre (*CF*)	2.29	0.19
Van Soest analysis (%, bs)		
Van Soest solubles (*VSs*)	39.35	(*)
hemicellulose (*h*)	56.48	(*)
cellulose (*c*)	3.46	(*)
lignin (*l*)	0.59	(*)
Van Soest ash (*VSa*)	0.12	(*)

N = 2, db = dry basis; wb = wet basis; NDF = Neutral Detergent Fibre; ADF = Acid Detergent fibre; ADL = Acid Detergent Lignin; (*) calculations as follows: *DM* = 100%-*M* (Eq. 42); *NFE* = 100%-*A*-*CP*-*CL*-*CF* (Eq. 43); *VSs* = 100%-*NDF* (Eq. 44); *h* = *NDF*-*ADF* (Eq. 45); *c* = *ADF*-*ADL* (Eq. 46); *l* = *ADL*-*VSa* (Eq. 47).

Drying kinetics and qualitative analysis using drying rate, desorption and effective diffusivity curves

Figures 1(a) and (b) show the drying curves of cassava root slices of 5- and 6-mm thicknesses, respectively, in terms of X_t / X_0 average of the triplicates *versus t*, at the seven temperatures studied. A detail of the end of the curves can be seen in the right upper corner, and the limit of the drying represented by storage moisture of 12% in a wet basis, approximately. Repeatability between replicates was in the range of 1.47 ± 1.35%, and 0.97 ± 0.72% for 5- and 6-mm thicknesses, respectively, which demonstrated the precision of the kinetic experiments. The curves show the monotonic decrease characteristic of the drying process. In the upper detail, the beginning of the dynamic pseudo-equilibrium stage can be observed (below the typical storage moisture of 12% in a wb, represented by X_S / X_0 in Figures 1(a) and (b), and equivalent to 0.0822) separating the kinetic stage from the superficial thermodynamic stage and characteristic of the real equilibrium. It is worth pointing out the importance of identifying the moisture content when reaching the dynamic pseudo-equilibrium (X_{dpe}) to guarantee an excellent behaviour of the kinetics drying models during the design and simulation of industrial-scale dryers. The mean values of X_{dpe}, for the temperatures from 55 to 105°C, were 0.1039, 0.0856, 0.0897, 0.0725, 0.0612, and 0.0546 $kg_{water} \cdot kg_{DS}^{-1}$, respectively. Predicted equilibrium moisture content, was then calculated with the data shown in Best (1978) and with de procedure suggested by Moreno *et al.* (2014) resulting in 0.0613, 0.0543, 0.0490, 0.0449, 0.0415, and 0.0388 $kg_{water} \cdot kg_{DS}^{-1}$, respectively. These values represent differences between 41 and 21% with respect to the real limit of the stage where diffusional phenomena predominate, represented by X_{dpe}.

It could be observed that the curves joined progressively as the drying temperature was increased in most of the cases; however, there were some exceptions. This could be attributable to the complexity involved when conducting an experiment of this nature. Among the conditions that are difficult to guarantee is diffusion homogeneity; in fact, the speed diffusion of water varies differently depending on the relative exposition of each face to the main

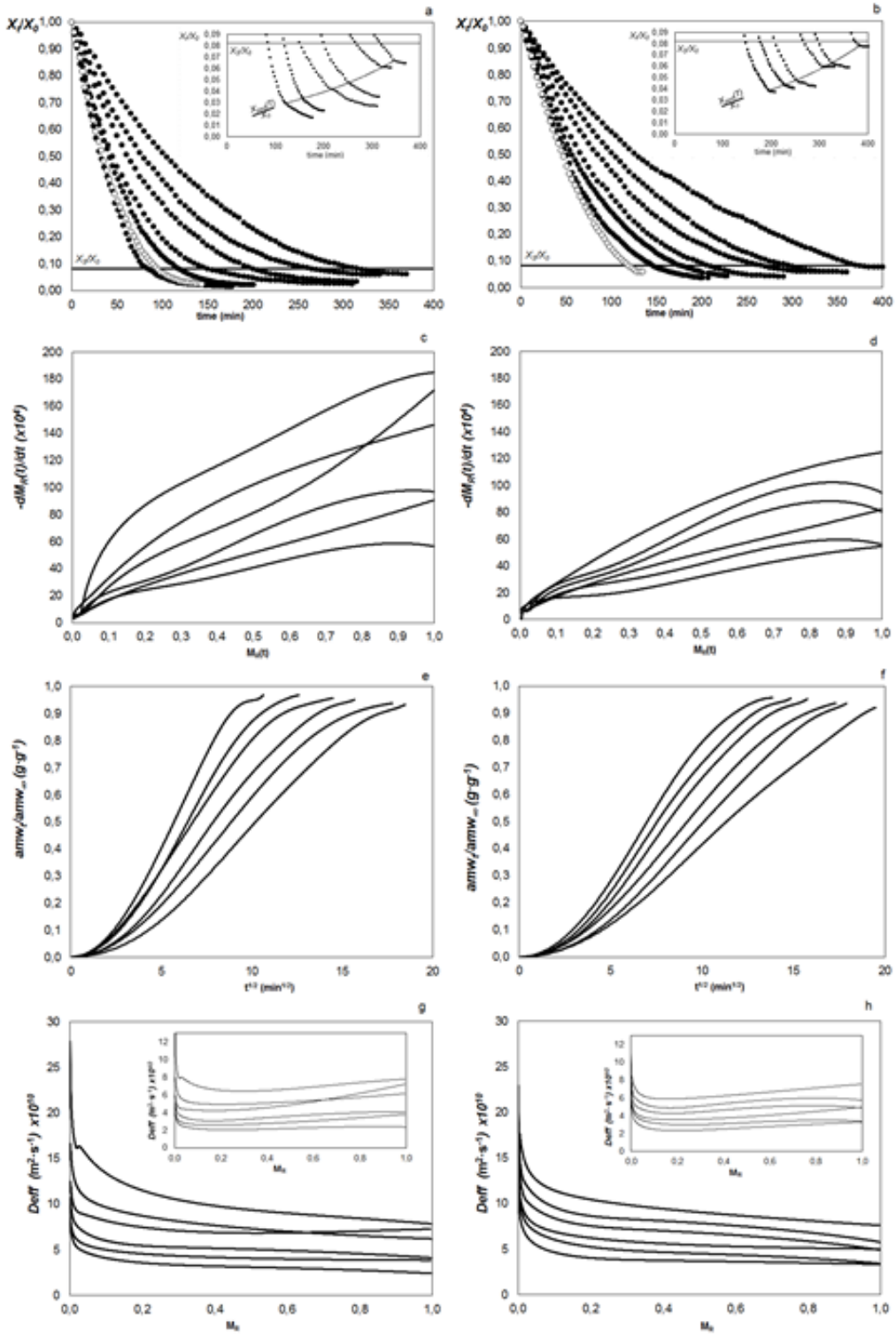

Figure 1. Experimental drying kinetics curves for cassava slices of (a) 5-mm, (b) 6 mm layer height; smoothed drying rate curves for cassava slices of (c) 5 mm and (d) 6 mm of layer height; smoothed water desorption curves for cassava slices of (e) 5 mm and (f) 6 mm of layer height; smoothed effective diffusivity curves for cassava slices of (g) 5 mm and (h) 6 mm of layer height.

stream of the hot air. There is also the fact of the inherent heterogeneity (anisotropy) of the material, and the changes that it may suffer during storage. This may influence the performance of the kinetic models and/or the correspondence or not of their parameters with respect to temperature.

It was observed, in turn, that the curve of 115°C, partially overlapped (6 mm) or decreased more slowly than that of 105°C (5 mm), which evidenced the occurrence of changes in cassava that decreased water desorption. This phenomenon could be hampering water diffusion through shrinkage and

collapse of the starch structure, thus decreasing the porosity of the material, and hence, the drying rate (Marousis *et al.,* 1991). Chemically speaking, the occurrence of amylopectin gelatinisation and/or dextrinisation, could have affected the drying process, so it makes no sense to model this temperature excluding a mathematical component that is adjusted according to the prevailing processes, nor including it, within the qualitative analysis of diffusional phenomenology, for the same reasons.

Figures 1(c) and (d) show the drying rate curves of cassava root slices of 5- and 6-mm thicknesses, respectively. It could be observed that the drying process took place in a single stage of decreasing drying rate with internal control, with a short initial adjustment period, not observing any stage of constant drying rate. The crossovers seen in some pair of curves are only the mathematical result of the derivation of the smoothing equations, but not a real intersection. The curves of 5 mm were obviously faster than those obtained for the 6 mm slices; a similar result was also obtained by Salgado *et al.* (1994).

Carranza and Sánchez (2002) reported a period of constant drying rate, which differed from the results of the present work. However, starch-rich tubers normally present an absence of constant rate period of drying (Prakash *et al.,* 2004; Yadollahinia and Jahangiri, 2009; Doymaz, 2011; Ju *et al.,* 2016). Diamante and Munro (1993) reported a contradictory result in the drying of sweet potato slices in an indirect solar dryer, in which they found a long constant rate period of drying in contrast with a previous work, where the same authors found an absence of this period for the same material but in a forced convective dryer. Salcedo *et al.* (2014) found a very short period of constant rate drying in cassava roots slices in a different cultivar from the one used in the present work. In addition, drying conditions reported by Carranza and Sánchez (2002) were not gentler due to the very high linear air speed employed. Considering these facts, the presence or absence of a constant rate period in the drying of cassava roots could be associated to a variety-based dependence. An important factor associated to handling conditions, not often reported in literature, should not be neglected because that could affect the free water content and thus, the constant rate period of drying.

Desorption curves for 5 and 6 mm, observed in Figures 1(e) and (f), respectively, present a sigmoidal shape showing the anomalous diffusion of water pattern as described by Crank (1975). That agrees with the observed drying rate curve, where an internal control governs the diffusion of water, due to the interaction with the predominant hydrophilic biopolymer matrix (starch). This behaviour is clearly anomalous, or non-fickian, verifying the beginning of the curve that is clearly sigmoidal, as well as the end. The partial straightness of the curves in its central part is not a sign of fickianity. The fickian or pseudo-fickian behaviour is given by a proportional beginning of the desorption curve, which is absent in these curves.

In Figures 1(g) and (h), effective diffusivity curves for 5- and 6-mm slices, respectively, are shown. Both curves are similar in values and shapes. Clearly, effective diffusivity did not have a linear horizontal behaviour, but rather a potential behaviour that induced one to affirm that diffusion of water during the drying of cassava roots is non-fickian, as demonstrated by the desorption curves. A linear adjustment reported an average coefficient of determination (R^2) for all curves of 62.39 ± 8.42%, while R^2 for a potential adjustment was 98.33 ± 1.26%, demonstrating the difficulties arising when trying to model and explain the phenomenology of the drying process using the energy of activation and, conversely, the easy way to compare fickianity and water affinity of different materials with this new tool. In the right upper corner are the families of effective diffusivity curves calculated with the expression of shrinkage suggested by Hernández-Pérez *et al.* (2004). A more complex behaviour can be seen, being the R^2 for linear adjustment of 9.83 ± 21.49, demonstrating the existence of a non-fickian diffusional process. Comparing the average power of the family curves of cassava roots (-0.1529), without the shrinkage expression, with other materials (Faneite, 2010), it can be said that the drying of cassava roots have more fickianity with respect to sugar cane bagasse (-0.3399), duckweed (-0.2153), and midrib of plantain leaves (-0.2088); similar fickianity with respect to plantain leaves (-0.1449) and cassava leaves (-0.1228); and less fickianity with respect to sugar cane (-0.0492) and yellow corn foliage (-0.0711). Setting out a hypothesis to explain these differences is out of the scope of this work, but it could be attributed to differences in the nature and composition of the present polysaccharides, shape and rigidity of the structure, original localisation of the water inside the vegetable matrix, para-crystallinity of cellulose or starch, porosity, anti-dehydration defences, etc.

Complementary quantitative analysis of phenomena involved in drying process with the use of XRD and FTIR

As can be seen in Figure 2(a), FTIR spectra

from dried cassava root samples showed the following characteristic signals of native starch: near 765 and 862 cm^{-1} corresponding with the C-C bond stretching, and the C-H bond vibration in starch structure; in the 900 - 1500 cm^{-1} range, bands at 930, 997, 1014, 1082 and 1159 cm^{-1} associated with -C-O-C- bonds from the anhydroglucose unit; the 1648 cm^{-1} band associated with the starch-linked water; and the 2923 and 3421 cm^{-1} bands associated with the C-H and –OH bonds vibrations (Solorzano *et al.,* 2011).

Figure 2(b) shows the same FTIR spectra showed in the previous Figure, plotted in terms of absorbance, in the 1200 - 600 cm^{-1} interval. A noticeable difference could be observed in the 997 cm^{-1} band: as temperature increased, absorbance decreased when the cassava root samples dried out at the highest drying temperatures. It could be concluded that glycosidic bonds α-(1→4) and probably α-(1→6) could have suffered a partial breaking, giving origin to dextrins, as stated by Aristizábal Galvis *et al.* (2007). Figure 2(a) (crystallinity index *versus* temperature) shows that the drying temperature affected the starch structure of the cassava root, increasing the proportion of amorphous structure as compared to the original crystalline structure, something compatible with the calculated wavelength band ratio at 1045 and 1014 cm^{-1} (originally was 1022 cm^{-1} but this band slightly moved to 1014 cm^{-1}) as described by several authors (Smits *et al.,* 1998; Branen *et al.,* 2002).

Figure 2(c) shows the XRD patterns of cassava root starch dried at different temperatures. It can be seen that this kind of starch had an A-type diffraction pattern, given the diffraction peaks at 2θ angles of 15, 17, 18 and 23° (Martín and López, 2009). Crystallinity index as a function of the temperature (upper right part of Fig 2(c)), confirmed that a crystallinity loss occurred with the increase of the drying temperature, and a consequent transition to an amorphous state of the starch granule (Martín and López, 2009). This decrease of the crystallinity was clearly higher between 95 and 115°C.

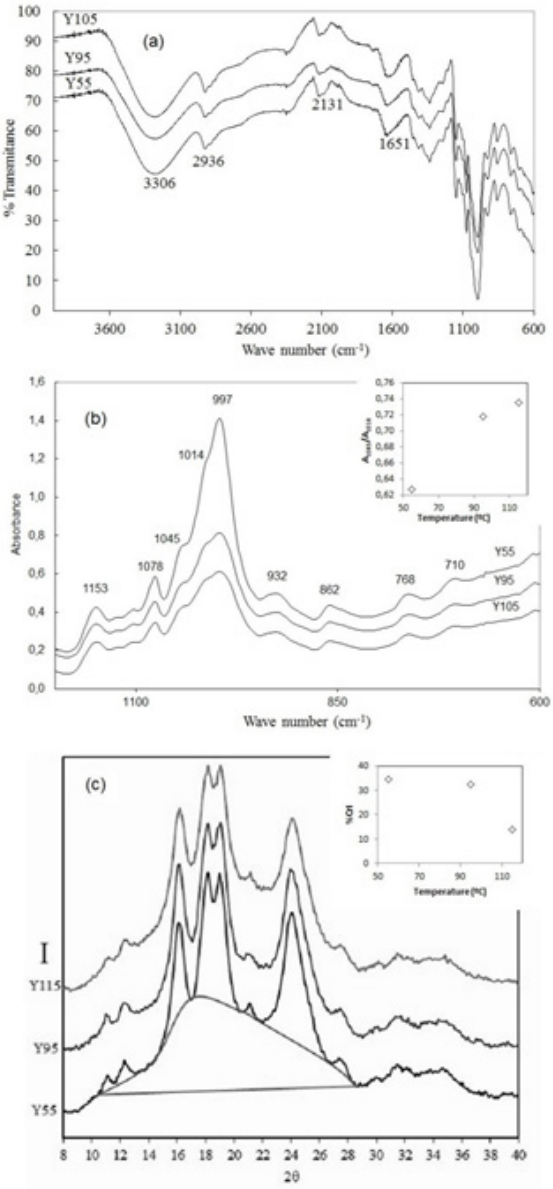

Figure 2. Cassava root starch (a) FTIR spectrum in terms of transmittance at 55, 95, and 115°C; (b) FTIR spectrum in terms of absorbance at 55, 95, and 115°C, and detail in the upper right of the ratio of absorbances of 1045 cm^{-1}/1014 cm^{-1} *versus* temperature; (c) XRD at 55, 95, and 115°C, and detail in the upper right of % CrI *versus* temperature.

Modelling of thin layer drying kinetics

Calculation of the empirical Eq. 17 - 25 showed that parameter *a* of Exponential of two terms (Eq. 18), Approximate diffusion (Eq. 19) and Verma (Eq. 20) models was not significant, being assigned a value of 0 by the GRG Method, thus being converted into the Newton equation. For this reason, these three models were discarded. Modified Page equation was discarded too, because the errors obtained by means of the least square method were equivalent to those of the original Page model. Parameter *a* of the original Faneite-Suárez model, truncated in the proportional term, was not significant for GRG, converting it into Page model. For this reason, Modified-Faneite-Suárez model was finally configured, putting different powers in both terms of the Equations. Modified-Faneite-Suárez thin-layer drying kinetics model finally had the following form:

$$M_R = a \cdot e^{-k \cdot t^n} + (1 - a) \cdot e^{-g \cdot t^m} \qquad \text{(Eq. 42)}$$

where, M_R = moisture fraction; t = time; *a, g, k, n* and *m* = adjustment parameters of the Faneite-Suárez equation.

In Table 2 are shown the parameters of Modified-Faneite-Suárez and Gauss models as the best empirical equation tested in the present work. In both cases, all the parameters had significance for GRG, but parameter *k* for Modified-Faneite-Suárez, did not reach statistical significance in some of the drying temperatures. We then decided not to eliminate it because Modified-Faneite-Suárez model without *k* converts into Page model but having a better performance with respect to it. This affirmation is supported by the results of the application of ANOVA and LSD methods on analytical statistical criteria of tendency, the experimental behaviour (R^2 and η_m) and model bias (*RMSE* and χ^2) (Table 2). The parameters of the winner models did not appear to be affected by temperature, confirming the presumption affirmed when kinetics behaviour was analysed in the drying curves.

Empirical and semi-theoretical models were proved in the same ANOVA and LSD study. Results of criteria using the traditional Crank Solution of Second Fick Law (Crank model), with the energy of activation as its main parameter, had to be excluded, as their results were very poor, not allowing to discriminate between the rest. Considering all the criteria analysed, Modified-Faneite-Suárez was the best, followed by Gauss model. Faneite-Mosquera model was combined with the X_{dpe} model to allow the direct calculation of X_t needed for the simulation program, adding an additional truncation error. Nevertheless, it was not the worst model (excluding results of Crank model with E_a). Parameters of Faneite-Mosquera model (Eq. 36) can be calculated using Eq. 43 - 46.

$$b = 1{,}0000x10^{-11} \cdot T(ºC) - 2{,}8897x10^{-10} \quad \text{(Eq. 43)}$$

$$m_{55-85ºC} = -7{,}5486x10^{-13} \cdot T(ºC) - 4{,}0642x10^{-11} \quad \text{(Eq. 44)}$$

$$m_{85-105ºC} = -4{,}7932x10^{-12} \cdot T(ºC) + 3{,}0276x10^{-10} \quad \text{(Eq. 45)}$$

$$X_{dpe}/X_0 = 0{,}1674 \cdot e^{-0{,}01534 \cdot T(ºC)} \quad \text{(Eq. 46)}$$

Figures 3(a) and (b) show the experimental points of the drying curve, in terms of M_R, with respect to Modified-Faneite-Suárez model, as a continuous line, for 5- and 6-mm slices, respectively. The extraordinary performance of this model was evident. Figures 3(b) and (c) show the experimental points of the drying curve, in terms of X_t / X_0, with respect to Faneite-Mosquera model, as a continuous line, for 5- and 6-mm slices, respectively. Indeed, a lesser performance was observed, with respect to the best model, but it can also be seen to be a logical and progressive behaviour with the increase of the drying temperature of predicted curves. Figures 3(d) and (e) show the residuals of M_R of Modified-Faneite-Suárez model, for 5- and 6-mm slices, respectively. A random distribution of residuals around 0, and a bias of ± 0.010 can be observed. Figures 3(g) and (h) show the residuals of X_t / X_0 of Faneite-Mosquera model, for 5- and 6-mm slices, respectively. Some tendencies of the residuals above and below 0, and a bias of ± 0.045 can be observed, being approximately of the same order of magnitude as the winner model.

Kajuna *et al.* (2001) obtained R^2 between 99.9 and 97.3% for the models evaluated (Newton and Page), falling below the performance of the Modified-Faneite-Suárez model (Table 2). Hernández-Pérez *et al.* (2004) obtained a RMSE for their model, based on a neural network of three neurons in the hidden layer (21 weights and 5 bias) of 0.0552, which is only lower than result of Crank model using energy of activation as main parameter (Table 2), and restricted to their experimental conditions (air temperature, air velocity, shrinkage, time, and air humidity) due to the high empiric character of a neural network approach. Salcedo *et al.* (2014) obtained R^2 of 97.55% (in accordance with the result of the Crank model using energy of activation as main parameter, presented in Table 2) and an average RMSE of 0.020 (close of Faneite-Mosquera model result, presented in Table 2) for their best model (Approximate diffusion). The correlation of effective diffusivity with respect to gas velocity and temperature affected the Crank Model approach, thus yielding a very low value of R^2 of 79.17%.

Conclusion

Cassava roots are an excellent source of energy in tropical countries but need to be dried for storage in industrial scale applications due to their high moisture content. Experimental drying curves, between 55 and 105°C, showed a monotonic decreasing of the moisture content, with a progressive approach, as the drying temperature increased. The drying process was followed by a transition state where the changes in the moisture content were very small. This point separated the kinetic stage from the superficial thermodynamic stage, characteristic of the real equilibrium which began in moisture content, under the traditional storage moisture content and above the equilibrium moisture content. Drying rate, water desorption, and effective diffusivity curves demonstrated that the transport of water through the cassava matrix in the drying process was controlled

Table 2. Faneite-Suárez modified and Gauss models parameters, and analytical statistical criteria of all models.

T (ºC)	*a*	*k*		*n*	*g*	*m*	*a*	*k*		*n*	*g*	*m*
55	0.2737	7.183E-08		3.0609	0.0048	1.1886	0.2260	2.416E-11		4.3199	0.0039	1.1778
65	0.3939	3.154E-05		2.0530	0.0126	1.0674	0.2718	2.257E-08		3.2857	0.0045	1.2085
75	0.1842	4.584E-08	ns	3.3359	0.0081	1.1675	0.3819	1.122E-05		2.2307	0.0102	1.0978
85	0.2713	4.681E-05	ns	2.1944	0.0248	0.9784	0.1646	2.476E-08	ns	3.4365	0.0063	1.2014
95	0.5165	2.979E-04	ns	1.8869	0.0263	1.0698	0.1499	5.126E-09	ns	3.8357	0.0074	1.1985
105	0.2770	3.505E-06	ns	3.0578	0.0211	1.1283	0.3373	3.832E-05	ns	2.2026	0.0138	1.1411

Gauss model parameters (L=5 mm)				***L = 6 mm***		
T (ºC)	***a***	***b***	***c***	***a***	***b***	***c***
55	1.6617	178.67	177.28	2.2117	315.27	250.22
65	2.5972	230.78	167.03	1.5966	164.52	170.08
75	2.8453	204.71	141.55	2.0536	194.19	161.87
85	4.4740	204.39	118.07	2.1204	164.14	133.88
95	1.6707	75.12	74.15	2.2194	149.53	118.42
105	1.3872	40.61	50.19	1.8468	103.89	93.33

Models	*Tendency of the models to copy the experimental behaviour (100% is perfect)*				*Model bias with respect to experimental data (0 represent no bias)*			
	R^2 (%)		**η_m (%)**		**RMSE**		**χ^2**	
	Mean	**SD**	**Mean**	**SD**	**Mean**	**SD**	**Mean**	**SD**
Lewis o Newton	99.47^{e}	0.24	98.52^{d}	0.54	0.0350^{e}	0.0072	0.001296^{e}	0.000527
Page	99.74^{cd}	0.14	99.71^{bc}	0.15	0.0153^{cd}	0.0035	0.000255^{bcd}	0.000125
Modified-Faneite-Suárez	99.98^{a}	0.01	99.98^{a}	0.01	0.0038^{a}	0.0012	0.000017^{a}	0.000012
Logistic	99.8^{bd}	0.12	99.78^{ac}	0.12	0.0134^{bc}	0.0033	0.000200^{ac}	0.000106
Gauss	99.89^{ab}	0.09	99.88^{ab}	0.10	0.0096^{b}	0.0034	0.000109^{ab}	0.000082
Faneite-Mosquera + X_{dpe}	99.85^{bc}	0.11	99.46^{e}	0.39	0.0189^{d}	0.0072	0.000460^{d}	0.000305
Crank Model using E_a	97.56	0.72	93.07	2.59	0.0756	0.0156	0.006160	0.002401

ns = non-significant parameters ($p < 0.05$, with 95% of confidence), $^{a\text{-}e}$groups with significant differences (95% of confidence), L = layer height, R^2 = coefficient of determination. *n* = efficiency of the model, RMSE = root mean square error, x^2 = Ji square, T = temperature.

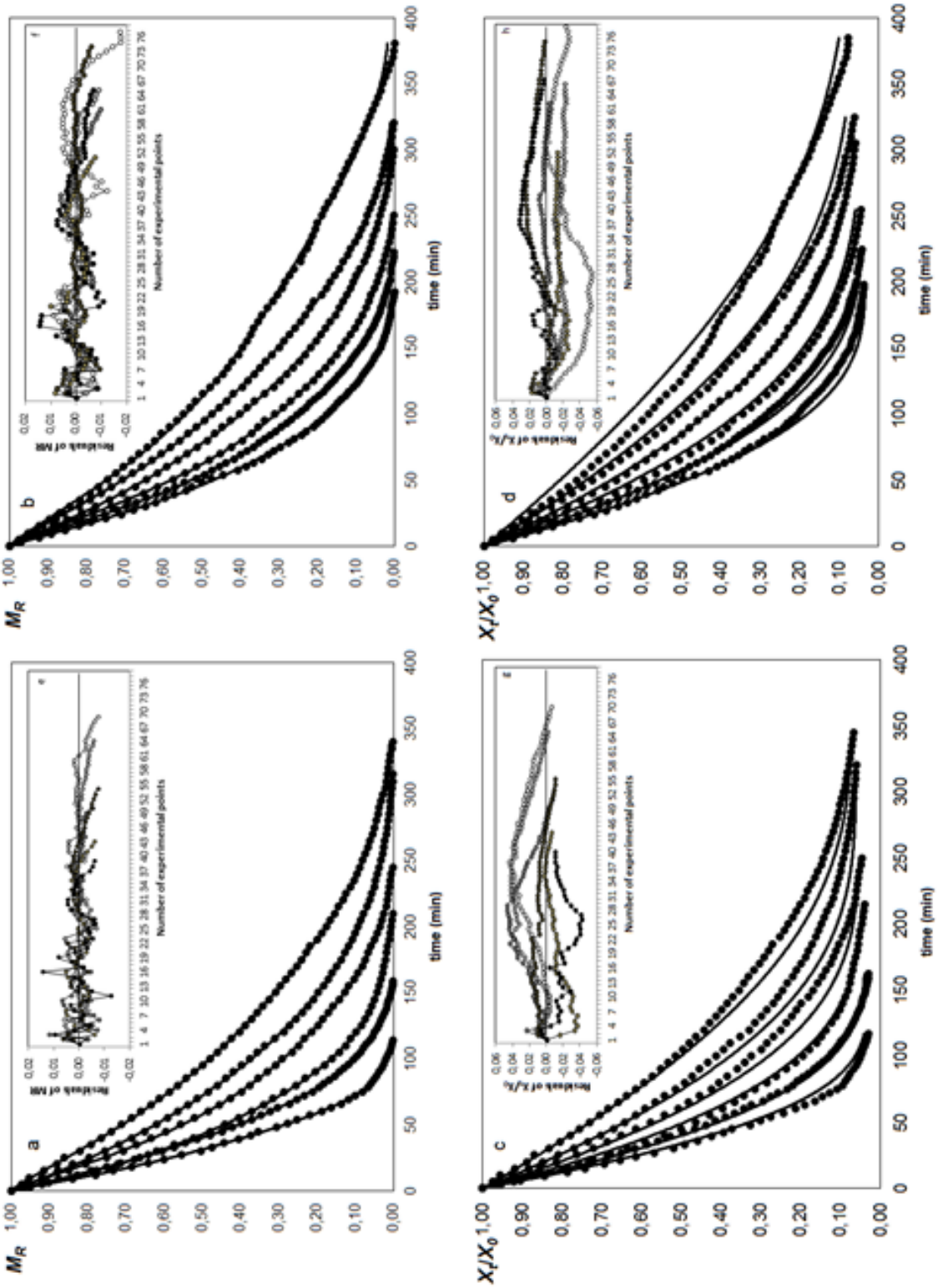

Figure 3. Drying kinetics data of cassava roots slices, for L = 5 mm (a) and 6 mm (b), in terms of M_R, and in terms of X_t/X_0, for L = 5 mm (c) and 6 mm (d). ● Experimental Data. - Faneite-Suárez modified model in Figures (a) and (b), and Faneite-Mosquera model in Figures (c) and (d). Residuals of M_R for L = 5 mm (e) and 6 mm (f), for Faneite-Suárez modified model, and of X_t/X_0, for L = 5 mm (g) and 6 mm (h), for Faneite-Mosquera model.

by internal forces, and the diffusion was anomalous. Changes in XRD patterns and FTIR spectra with the increase of the drying temperature, specifically between amorphous and crystalline regions, explained the excessive slowdown of the drying curve at 115°C, thus preventing its use in modelling of the drying process, with thin-layer drying kinetics models. The new model, Modified-Faneite-Suárez, has demonstrated a superior performance in the modelling of the thin-layer drying process of cassava roots whereas the new semi-theoretical model, Faneite-Mosquera, is recommended for process simulation purposes.

Acknowledgement

Special thanks to the staff of Zulian Technological Research Institute (INZIT) for their support in the FTIR and XRD measurements; to the Secretaría de Educación Superior, Ciencia y Tecnología e Innovación (SENESCYT) of the Republic of Ecuador for the financial support of Dr. Angós as Prometeo Researcher; to the Venezuelan research and development company SECAVENCA for its support in sampling and the use of computer tools for data modelling; and to Dr. Javier García Del Valle for his critical review of mathematical equations.

References

Aguerre, R. J. and Suarez, C. 2004. Diffusion of bound water in starchy materials: application to drying. Journal of Food Engineering 64(3): 389-395.

Association of Official Analytical Chemists (AOAC). 2000. Official methods of analysis of the Association of Official Analytical Chemists. 17th ed. United States: AOAC.

Aristizábal Galvis, J., Moreno, F. L. and Basto Ospina, G. 2007. Studying a new technique and implementing a pilot-line process for obtaining dextrins from cassava starch. Ingeniería e Investigación 27(2): 26-33.

Best, R. 1978. Cassava processing for animal feed. In Weber, E. J., Cock, J. H. and Chouinard, A. (eds). Cassava Harvesting and Processing: Proceedings of a workshop held at CIAT, Columbia. Ottawa: International Development Research Centre.

Branen, A. L., Davidson, P. M., Salminen, S. and Thorngate, J. H. 2002. Food additives. 2nd ed. New York: Marcel Dekker Inc.

Carranza, J. and Sánchez, M. 2002. Drying kinetics of *Musa paradisiaca* L. "plantain" and *Manihot esculenta* Crantz "cassava". Revista Amazónica de Investigación Alimentaria 2(1): 15-25.

Cheetham, N. W. H. and Tao, L. 1998. Variation in crystalline type with amylose content in maize starch granules: an X-ray powder diffraction study. Carbohydrate Polymers 36(4): 277-284.

Crank, J. 1975. The mathematics of diffusion. 2nd ed. Oxford: Clarendon Press.

Diamante, L. M. and Munro, P. A. 1993. Mathematical modelling of the thin layer solar drying of sweet potato slices. Solar Energy 51(4): 271-276.

Doymaz, İ. 2011. Thin-layer drying characteristics of sweet potato slices and mathematical modelling. Heat and Mass Transfer 47: 277-285.

Durango, N., Bula, A., Quintero, H. and Ferrans, O. 2004. Construction of a model of cassava dryer, in porous medium, using radial flow of hot air. Revista de la División de Ingeniería de la Universidad del Norte 15: 9-30.

Esmaiili, M., Sotudeh-Gharebagh, R., Mousavi, M. A. and Rezazadeh, G. 2007. Influence of dipping on thin-layer drying characteristics of seedless grapes. Biosystems Engineering 98(4): 411-421.

Faneite, A. 2010. Drying kinetics of lignocellulosic materials untreated and treated with pressurisation and depressurisation (PDA). Venezuela: University of Zulia, MSc thesis.

Faneite, A., Rincón, A., Ferrer, A., Angós, I. and Arguello, G. 2016. Mathematical modeling of thin layer drying of green plantain (*Musa paradisiaca* L.) peel. International Food Research Journal 23(5): 2088-2095.

Food and Agriculture Organization (FAO). 2017. Statistics data. Retrieved on September 22, 2018 from FAO website: http://www.fao.org/faostat/en/#data/QC

García, P., Cabrera, S., Sánchez, J. and Pérez, I. 2009. Corn yield and planting date at the western plains of Venezuela. Agronomía Tropical 59(2): 161-172.

Garzón, V. 2010. Cassava in monogastric feeding. Retrieved on September 22, 2012 from ERGOMIX website: https://www.engormix.com/avicultura/articulos/yuca-en-monogastricos-t28644.htm

Hernández-Pérez, J. A., García-Alvarado, M. A., Trystram, G. and Heyd, B. 2004. Neural networks for the heat and mass transfer prediction during drying of cassava and mango. Innovative Food Science and Emerging Technologies 5(1): 57-64.

Ju, H. Y., El-Mashad, H. M., Fang, X.-M., Pan, Z., Xiao, H.-W., Liu, Y.-H. and Gao, Z.-J. 2016. Drying characteristics and modeling of yam

slices under different relative humidity conditions. Drying Technology 34(3): 296-306.

Kajuna, S. T. A. R., Silayo, V. C. K., Mkenda, A. and Makungu, P. J. J. 2001. Thin-layer drying of diced cassava roots. African Journal of Science and Technology 2(2): 94-100.

Karim, M. A. and Hawlader, M. N. A. 2005. Drying characteristics of banana: theoretical modelling and experimental validation. Journal of Food Engineering 70(1): 35-45.

Marousis, S. N., Karathanos, V. T. and Saravacos, G. D. 1991. Effect of physical structure of starch materials on water diffusivity. Journal of Food Processing and Preservation 15(3): 183-195.

Martín, J. C. and López, E. 2009. Physical modification of cassava starch and evaluation of susceptibility to enzyme hydrolysis by alpha amylase. Revista Colombiana de Química 38(3): 395-408.

Mayor, L. and Sereno, A. M. 2004. Modelling shrinkage during convective drying of food materials: a review. Journal of Food Engineering 61(3): 373-386.

Morin G, H. A., Faneite N., A. M., Salones C., G. del V., Gamez G., J. V., and Ferrer O., A. de J. 2017. Biorefining of the *Prosopis juliflora* fruit for ethanol production. Evaluation of the conditioning and pretreatment stages. AVANCES Investigación en Ingeniería 14(1): 169-183.

Moreno, F. L., Parra-Coronado, A. and Camacho-Tamayo, J. H. 2014. Mathematical simulation parameters for drying of cassava starch pellets. Engenharia Agrícola 34(6): 1234-1244.

Nara, S. and Komiya, T. 1983. Studies on the relationship between water-saturated state and crystallinity by the diffraction method for moistened potato starch. Starch 35(12): 407-410.

Prakash, S., Jha, S. K. and Datta, N. 2004. Performance evaluation of blanched carrots dried by three different driers. Journal of Food Engineering 62(3): 305-313.

Salcedo, J., Mercado, J. L., Vanegas, M., Fernández, A. and Vertel, M. L. 2014. Drying kinetics of cassava (*Manihot esculenta* Crantz) variety CORPOICA M-tai depending on the temperature and air velocity. Revista ION 27(2): 29-42.

Salgado, M. A., Lebert, A., García, H. S., Muchnik, J. and Bimbenet, J. J. 1994. Development of the characteristic drying curve for cassava chips in monolayer. Drying Technology 12(3): 685-696.

Smits, A. L. M., Ruhnau, F. C., Vliegenthart, J. F. G. and van Soest, J. J. G. 1998. Ageing of starch based systems as observed with FT-IR and solid-state NMR spectroscopy. Starch 50(11-12): 478-483.

Solorzano, S., Balsamo, V. and Ehrmann, E. 2011. Chemical modification of cassava starch with maleic anhydride via microwaves. Revista Latinoamericana de Metalurgia y Materiales S3: 4-5.

United States Department of Agriculture (USDA). 2018. Venezuela: grain and feed annual. Retrieved on April 18, 2018 from USDA website: https://www.fas.usda.gov/data/venezuela-grain-and-feed-annual-2

Véliz, T., Valente, A., Valcárcel, L. and Noa, M. 2002. Detection of cyanide and comparison of two methods for its detoxification in cassava (*Manihot esculenta* Crantz). Revista CENIC Ciencias Químicas 33(1): 3-6.

Yadollahinia, A. and Jahangiri, M. 2009. Shrinkage of potato slice during drying. Journal of Food Engineering 94(1): 52-58.

Zomahoun, J. P. O. C., Arouna, A. and Megnanglo, M. 2005. Conception of a drier for the semi-industrial production of dried cassava. In Proceedings of the International Research on Food Security, Natural Resource Management and Rural Development (Tropentag 2005). Germany: University of Hohenheim.